ADVANCED FUNCTIONAL MATERIALS

FULL PAPER

DOI: 10.1002/adfm.200800492

Cadmium(II) (8-Hydroxyquinoline) Chloride Nanowires: Synthesis, Characterization and Glucose-Sensing Application**

By *Hongcheng Pan, Hongyu Lin, Qingming Shen,* and *Jun-Jie Zhu**

Luminescent cadmium(II) (8-hydroxyquinoline) chloride (CdqCl) complex nanowires are synthesized via a sonochemical solution route. The results of X-ray photoelectron spectroscopy, energy dispersive X-ray analysis, infrared spectroscopy, elemental analysis (EA), and atomic absorption spectroscopy demonstrate that the chemical composition of the product is $Cd(C_9H_6NO)Cl$. Transmission electron microscopy and scanning electron microscopy images show that the CdqCl product is wire-like in structure, with a diameter of approximately 50 nm and an approximate length of 2–4 μm. The morphology and composition of the product can be transformed from Cdq_2 micrometer-scaled flakes to CdqCl nanowires by increasing the ratio of $CdCl_2$/q. A new fluorescent sensing strategy for detecting H_2O_2 and glucose is developed and is based on the combination of the luminescent nanowires and the biocatalytic growth of Au nanoparticles. The quenching effects of Au nanoparticles and $AuCl_4^-$ on the fluorescence of CdqCl nanowires are investigated. The dominant factor for the fluorescence quenching of CdqCl nanowires is that the Stern–Volmer quenching constant of Au nanoparticles is larger than that of $AuCl_4^-$.

1. Introduction

Metal 8-hydroxyquinoline (Mq_n) chelates have been the focus of many studies because of their wide range of applications in photoluminescence, electroluminescence, and field-emission. Anzenbacher and co-workers recently reported the synthesis of a series of emission-color-tunable Alq_3 complexes with arylethynyl substituents.[1] The substituents were found to affect the emission color and fluorescence quantum yield of the resulting Al^{III} complex. A new δ-phase of Alq_3 was identified and its blue luminescence studied.[2,3] Brett and co-workers fabricated chiral thin films, consisting of submicrometer scaled helical Alq_3 structures that generate circularly polarized photoluminescence.[4] As electroluminescent materials, Mq_n and its derivatives have been widely used in organic light-emitting devices (OLEDs).[5–10] Alq_3 has been used frequently because of its good electronic conductivity and strong electroluminescence emission.[11,12] Many other Mq_n chelates have also been demonstrated to be useful emitter materials. For instance, the Gaq_3 devices have a power efficiency that is approximately 50% higher than Alq_3 structures, suggesting that Gaq_3 might be a superior emitter material for display applications. The operating voltage of $(Znq_2)_4$-based OLEDs is lower than that of identical devices made with Alq_3.[6] Due to the unique optoelectronic properties of nanostructured organic materials, more attention is, therefore, turning to nanostructured Mq_n chelates. For example, the electroluminescent device fabricated by Alq_3 nanowires showed an obvious size-dependent performance.[5] In addition, Alq_3 nanostructures, such as nanowires, nanorods, and nanometer-scaled crystalline films, exhibited field emission with a relatively low turn-on voltage.[13–15] Currently, most research work has focused on the nanostructure of Alq_3 and Znq_2. Only a few investigations of other metal 8-hydroxyquinoline nanostructures have been carried out, partly because it is not easy to synthesize a well-defined nanostructure.

Recently, luminescent Cdq_2 has received much attention. As most-frequently reported in the literature, Cdq_2 can be synthesized by the reaction of the cadmium ion with excess 8-hydroxyquinoline.[16,17] For instance, Cdq_2 nanorods and nanoflowers were synthesized in an oleic acid/sodium oleate/ethanol/hexane/H_2O system at a Cd^{2+}/q ratio of 1:2.[18] The reaction time, temperature, and reagent concentrations are the key factors in controlling the morphology of the Cdq_2 nanostructure at a q-excess condition. However, it is interesting to investigate the situation where q reacts with excess cadmium salt. A new structure might be obtained because of the effect of the cadmium-salt anion on the formation of Cdq_2.

Herein, we report a sonochemical route to synthesize well-defined CdqCl nanowires in the presence of a highly excessive amount of cadmium salt ($CdCl_2$), while Cdq_2 flakes were obtained at a q-excess condition. By increasing the ratio of $CdCl_2$/q, the morphology and composition of the products could be transformed from Cdq_2 micrometer-scaled flakes to CdqCl nanowires. Furthermore, the prepared CdqCl nanowires can be developed into a fluorescence sensor for H_2O_2 and

[*] Prof. J. J. Zhu, Dr. H. C. Pan, H. Y. Lin, Q. M. Shen
Key Lab of Analytical Chemistry for Life Science (MOE)
School of Chemistry and Chemical Engineering
Nanjing University, Nanjing 210093 (P. R. China)
E-mail: jjzhu@nju.edu.cn

[**] This work is supported by the National Natural Science Foundation of China (NSFC; No. 20325516, 20635020, 90606016), NSFC for Creative Research Group (No. 20521503), and the China Scholarship Council (No. 20073020). We also thank the support of the National Basic Research Program of China (2006CB933201).

ADVANCED FUNCTIONAL MATERIALS

glucose, based on biocatalytic growth of Au nanoparticles. The quenching effects of Au nanoparticles and $AuCl_4^-$ on the fluorescence of CdqCl nanowires were investigated. Accordingly, a model was proposed to describe the mechanism of the fluorescence quenching of CdqCl nanowires. The results demonstrate that the difference in the respective Stern–Volmer quenching constants of the two quenchers ($AuCl_4^-$ and generated Au nanoparticles) plays the most importance role in the change of total fluorescence intensity.

2. Results and Discussion

2.1. Product Composition and Morphology

The composition of the CdqCl nanowires was confirmed by elemental analysis (EA), atomic absorption spectroscopy (AAS), and energy dispersive X-ray (EDX) spectroscopy. The results of EA and AAS show that the content of C, H, N, and Cd is 37.11, 2.01, 4.81, and 37.84%, respectively. The EDX spectrum in Figure 1a shows very strong peaks for Cd and Cl. The atomic ratio of Cd/Cl is 1.09:1. These results are in good agreement with the theoretical values (calculated for $Cd(C_9H_6ON)Cl$: C: 37.02%, H: 2.07%, N: 4.80%, Cd: 38.49%; the Cd/Cl atomic ratio was 1:1).

The IR spectrum of the CdqCl nanowires in Figure 1b does not show any strong band in the region from 4000 to 2000 cm^{-1}, indicating no OH vibrations are detected. In the IR region between 1600 and 700 cm^{-1}, the peaks are attributed to the quinoline ligand vibrations. The vibrations of Cd–ligand and Cd–Cl bonds are observed in the region between 700 and 100 cm^{-1}. The detailed assignments are summarized in Table 1.[16,19–21]

Figure 1c shows X-ray photoelectron spectroscopy (XPS) of the CdqCl nanowires. Detailed spectra were taken at the Cd and Cl regions, as shown in the insets of Figure 1c. The binding energy values of Cd $3d_{3/2}$, Cd $3d_{5/2}$, and Cl $2p_3$ are 412.7, 405.7, and 199.2 eV, respectively.

The morphology of the CdqCl nanowires was studied by transmission electron microscopy (TEM) and scanning electron microscopy (SEM). Figure 2 shows that the typical CdqCl nanowires are about 30–50 nm in diameter and about 2–4 μm in length. When the $CdCl_2$/q ratio was changed from 3:1 to 10:1, no significant changes in the diameter and length were observed. However, an increase of the reaction time from 50 to 120 min resulted in a slight increase in the diameter. Although an increase of the $CdCl_2$/q ratio from 3:1 to 10:1 showed quite limited effects on product morphology, significant changes were seen when the ratio was decreased from 1:1 to 1:5. The products synthesized at the 1:5 ratio have a flake-like morphology and a wide particle size distribution from hundreds of nanometer to thousands of nanometers, as shown in Figure 3a and b. The as-prepared products were characterized by EA, AAS, and XPS. The C, H, N, and Cd content is 53.97, 3.07, 6.86, and 29.73%, respectively. The results are in good agreement with the molecular formula for Cdq_2: $Cd(C_9H_6ON)_2$, C: 53.95%, H: 3.02%, N: 6.99%, Cd: 28.05%.

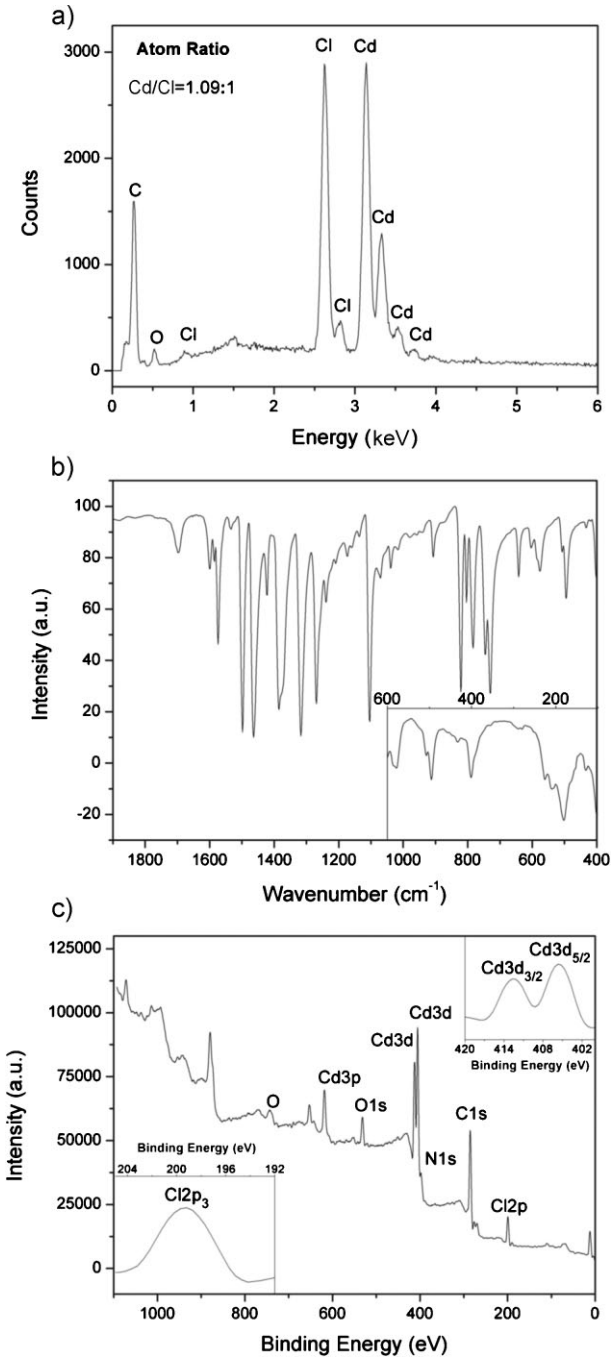

Figure 1. Spectral measurements of CdqCl nanowires: a) EDX spectrum, b) infrared (IR) spectra, inset: Far-IR spectrum, c) X-ray photoelectron spectroscopy (XPS) analysis, inset: high-resolution XPS in the Cd 3d (top-right) and Cl 2p (bottom-left) regions.

Furthermore, from the XPS result, no Cl peak was observed. Thus, the composition of prepared samples was confirmed as Cdq_2. An increase of the $CdCl_2$/q ratio to 1:3 and 1:1 led to observation of wire-like nanostructures in the TEM images. By further increasing the $CdCl_2$/q ratio to 3:1, the flake-like particles disappeared, and instead, a large number of nanowire structures were found. The wire-like morphology did not

Table 1. Wavenumbers and assignments of IR spectra of the CdqCl nanowires.

Wavelength [cm^{-1}]	Assignment	Wavelength [cm^{-1}]	Assignment
1599 and 1574	CC stretching vibration involving the quinoline group	783	out-of-plane CH wagging vibrations (quinoline groups)
1498 and 1464	CC/CN stretching and CH bending vibration	746	Ring breath/Cd–N stretching
1269	C–O, C–C stretching	731	Ring breath/Cd–N stretching
1240 and 1103	C–C,C–N stretching/C–H bending	642	Cd–O, Cd–N stretching/CCC bending
1039	CH bending and CC bending	578	CCC bending/Cd–N,Cd–O stretching
1016	C–H out-of-plane wagging	434	Cd–N stretching/CCC bending/Cd–O bending
906	CH out-of-plane wagging	401	Cd–N stretching/CCC bending
821	CH wagging (phenyl)	280	Cd–Cl stretching
804	CH wagging	181	CCCC twisting/butterfly

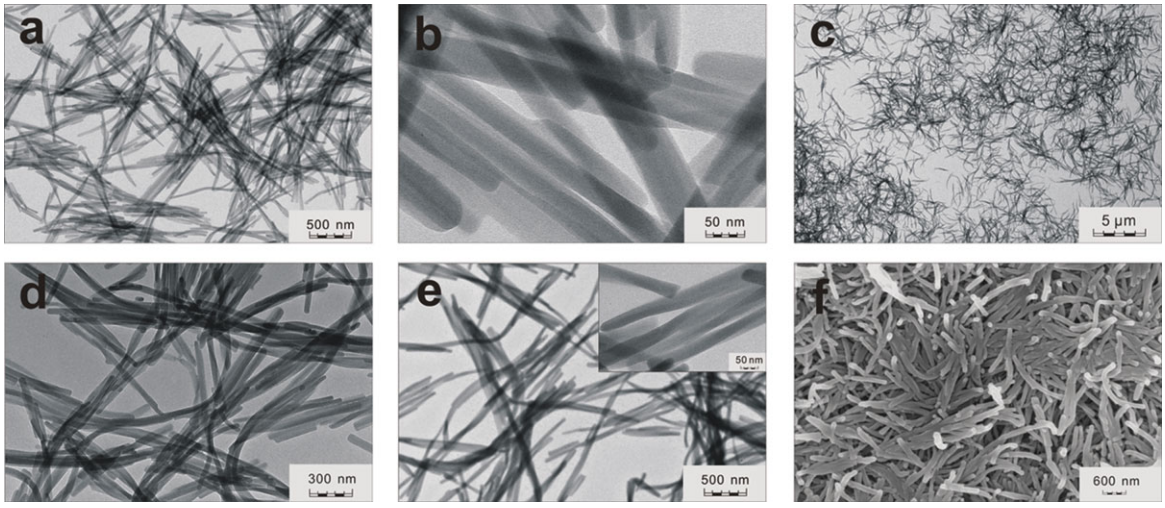

Figure 2. TEM images of CdqCl nanowires synthesized at $CdCl_2$/q ratios of a,b) 3:1, c,d) 5:1, e) 10:1. f) SEM image of CdqCl nanowires synthesized at a $CdCl_2$/q ratio of 3:1. The reaction times were a–e) 50 min and f) 120 min.

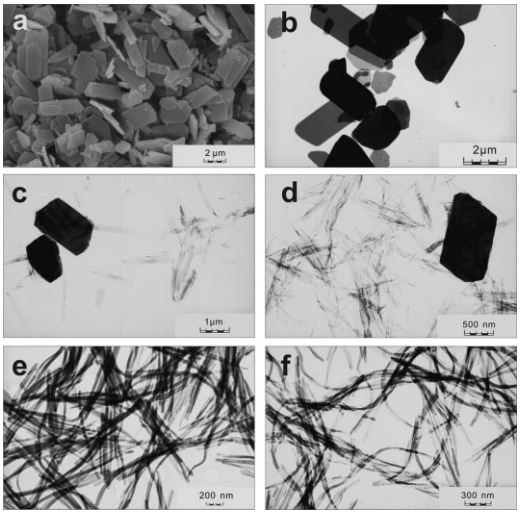

Figure 3. a) SEM image of the product synthesized at a $CdCl_2$/q ratio of 1:5. TEM images of the products synthesized at $CdCl_2$/q ratios of b) 1:5, c) 1:3, d) 1:1, e) 3:1, and f) 5:1. The reaction time was 50 min.

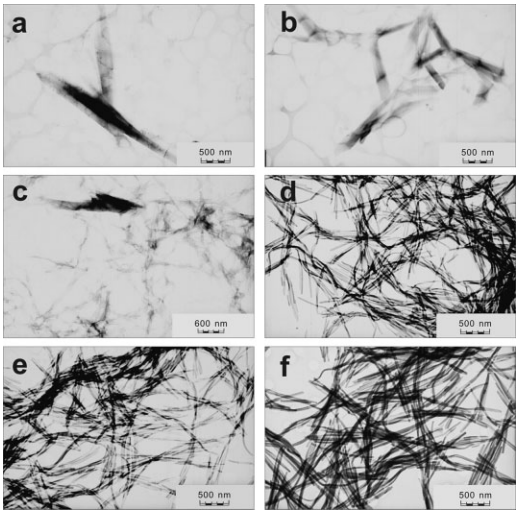

Figure 4. TEM images of the samples obtained at different reaction times: a) 2, b) 12, c) 20, d) 30, e) 50, and f) 120 min.

ADVANCED FUNCTIONAL MATERIALS

change even if the $CdCl_2$/q ratio increased to 10:1. The experiments support the conclusion that the composition of the product synthesized at a $CdCl_2$/q ratio of 1:5 is Cdq_2. This is consistent with the reported result that Cdq_2 could be formed when ligand q is present in excess. However, when the $CdCl_2$/q ratio was increased to 1:3 and 1:1, the products are a mixture of Cdq_2 and CdqCl, due to the coordination of Cl^- with Cd^{2+} to form CdqCl.

Time-dependent experiments were performed to investigate the formation process of the CdqCl nanowires. The samples obtained at a $CdCl_2$/q ratio of 3:1 were characterized by TEM at different reaction times. Figure 4 shows the TEM images taken from the reaction mixture after the solution was exposed to ultrasound irradiation for 2, 12, 20, 30, 50, and 120 min. Figure 4a shows that the initial products are shuttle-like structures with a size of 200 nm $\times$1 μm at a reaction time of 2 min. As the reaction time increases, the shuttle-like particles become thinner and slender. When the reaction time reached 20 min, nanowires were observed (Fig. 4c). At a reaction time of 30 min, the main morphology was nanowires (Fig. 4d). The fact that the shuttle-like structures transform to nanowires supports the supposition that the products undergo a recrystallization process. After 50 min, the wire-like morphology did not change with an increase of reaction time. We also carried out the reaction with electromagnetic stirring instead of ultrasound irradiation. At the $CdCl_2$/q ratio of 3:1, CdqCl nanowires were obtained without ultrasonic irradiation. However, using ultrasonic irradiation can obtain a more uniform morphology of CdqCl nanowires and can shorten the reaction time. TEM images of CdqCl nanowires obtained with and without ultrasonic irradiation are shown in Figure 5.

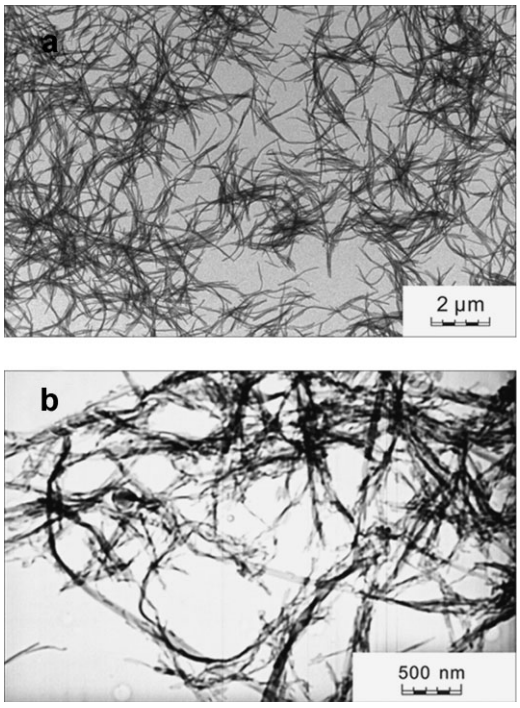

Figure 5. TEM images of the CdqCl nanowires obtained with a) ultrasound irradiation and b) electromagnetic stirring ($CdCl_2$/q = 3:1).

2.2. Fluorescence Sensing for H_2O_2 and Glucose

We used the CdqCl nanowires, combined with biocatalytically grown Au nanoparticles, to develop a fluorescence sensing strategy for H_2O_2 and glucose. Recently, Willner and coworkers developed an optical biosensor based on biocatalytically generated Au nanoparticles.[22–27] The excellent fluorescence properties of the CdqCl nanowires, when combined with biocatalytic growth of Au nanoparticles, allow us to develop a sensitive fluorescence sensing strategy for H_2O_2 and glucose.

Figures 6 and 7 show the fluorescence sensing for H_2O_2 and glucose by using CdqCl nanowires. The ways to generate Au nanoparticles for H_2O_2 and glucose sensing are different. In the case of H_2O_2, $AuCl_4^-$ could be reduced by H_2O_2 in the presence of Au nanoparticle seeds. In the case of glucose, the oxidase-biocatalyzed oxidation of glucose leads to the formation of H_2O_2, which acts

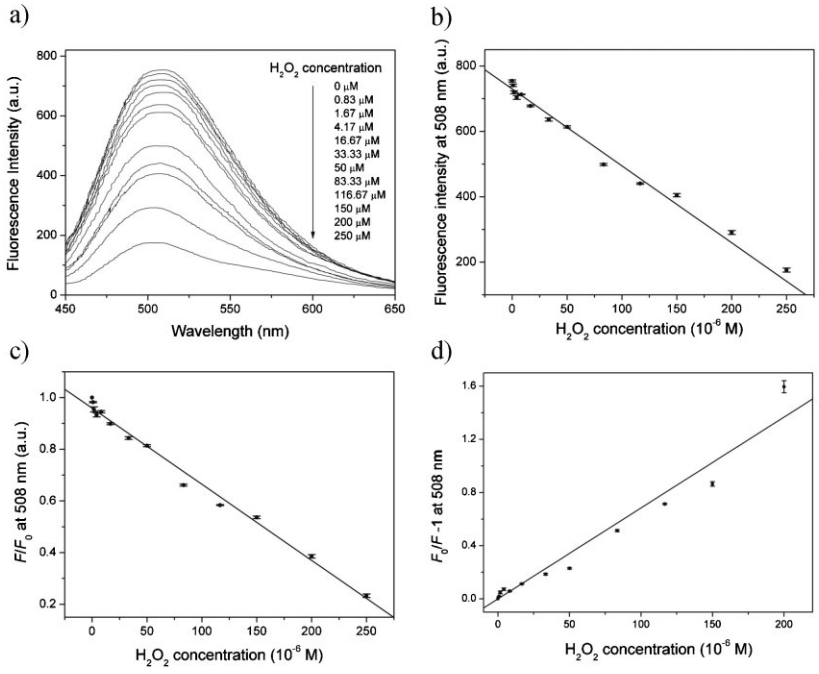

Figure 6. a) Variation in the fluorescence spectra of CdqCl nanowires mixed with 5 mL of the Au nanoparticles growth solution (containing 1.8×10^{-6} M Au seeds, 2.4×10^{-4} M $HAuCl_4$, 2.0×10^{-3} M cetyltrimethylammonium chloride (CTAC), 15 μL cysteamine, and 0.01 M phosphate-buffered saline (PBS), pH 7.05), reacting with different concentrations of H_2O_2. b) Fluorescence intensity at 508 nm versus H_2O_2 concentration. c) F/F_0 against H_2O_2 concentration (see Eq. 1 for definition of F and F_0). d) The S–V plot.

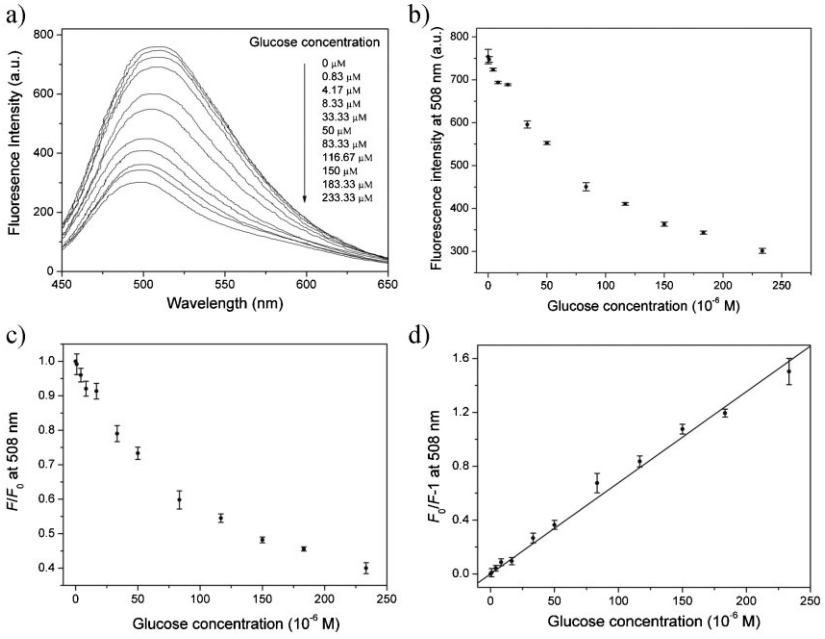

Figure 7. a) Variation in the fluorescence spectra of CdqCl nanowires mixed with 5 mL of the Au nanoparticles growth solution (containing 1.8×10^{-6} M Au seeds, 2.4×10^{-4} M $HAuCl_4$, 2.0×10^{-3} M CTAC, 47 μg mL^{-1} GOx (glucose oxidase), 15 μL cysteamine, 0.01 M PBS, pH 7.05), reacting with different concentrations of glucose. b) Fluorescence intensity at 508 nm versus glucose concentration. c) F/F_0 against glucose concentration. d) The S–V plot.

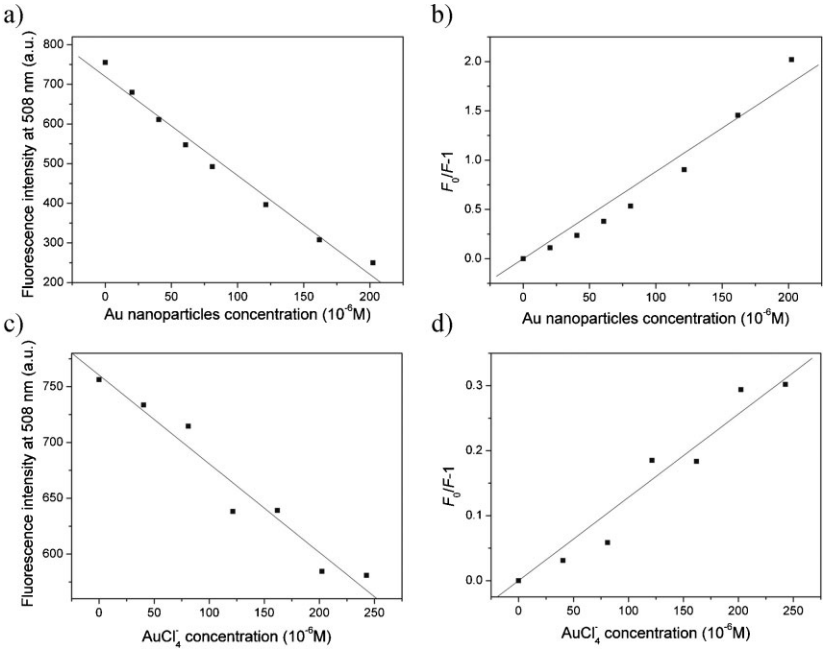

Figure 8. The fluorescence quenching of CdqCl nanowires by Au nanoparticles: a) the fluorescence intensity at 508 nm versus Au nanoparticle concentration, b) S–V plot. The fluorescence quenching of CdqCl nanowires by $AuCl_4^-$ nanoparticles: c) the fluorescence intensity at 508 nm versus $AuCl_4^-$ concentration, d) S–V plot.

as a reducing reagent for the generation of Au nanoparticles. Whatever the growth process for Au nanoparticles, the concentration of generated Au nanoparticles is dominated by the concentration of H_2O_2 or glucose. After the generation of Au nanoparticles, CdqCl nanowires were added to the growth solution. When the nanowires was added into the growth solutions with differently generated Au nanoparticle concentrations, the fluorescence of CdqCl nanowires was quenched with increasing Au nanoparticle concentration, as shown in Figures 6a and 7a.

Figures 6b and 7b show the calibration curve derived from the changes in the fluorescence at $\lambda = 508$ nm as the concentration of H_2O_2 and glucose, respectively, increases. The linear concentration ranges for H_2O_2 and glucose are from 8.33×10^{-7} to 2.5×10^{-4} M and from 8.33×10^{-7} to 2.33×10^{-4} M, respectively.

For understanding the mechanism of the fluorescence quenching, the effects of $AuCl_4^-$ and catalytically generated Au nanoparticles on the fluorescence of CdqCl nanowires were investigated. We synthesized Au nanoparticles by using H_2O_2 as a reducing reagent without glucose or glucose oxidase (GOx) in the growth solution, which contained 2.4×10^{-4} M $HAuCl_4$, 2.0×10^{-3} M CTAC, and 0.01 M PBS, at pH 7.05. The Au nanoparticles were collected to study the effect of the Au nanoparticles on the fluorescence of the CdqCl nanowires. Figure 8 shows the fluorescence intensities of CdqCl nanowires at various concentrations of catalytically generated Au nanoparticles or $AuCl_4^-$. The increasing concentration of Au nanoparticles or $AuCl_4^-$ leads to a decrease in the emission intensity of CdqCl nanowires. But no significant shifts were observed in the emission maximum. The possible quenching mechanism can be studied by determining the quenching rate parameters by means of Stern–Volmer (S–V) plots, which are drawn in accordance with the S–V equation:[28,29]

$$\frac{F_0}{F} = 1 + K_{SV}[Q] \quad (1)$$

where F_0 and F denote the steady-state fluorescence intensities in the absence and in the presence of quencher, respectively, K_{SV} is the Stern–Volmer quenching constant, and [Q] is the concentration of quencher. Figure 8b and d shows the S–V plots of the fluorescence quenching of CdqCl nanowires by Au nanoparticles and $AuCl_4^-$, respectively, and are found to be linear. K_{SV} for the Au nanoparticles and $AuCl_4^-$ are 8.84×10^3 and 1.28×10^3 M^{-1}, respectively. According to the results above, a model was proposed to explain the mechanism of the fluorescence quenching of CdqCl nanowires

ADVANCED FUNCTIONAL MATERIALS

by the biocatalytically grown Au nanoparticles. Assuming that the fluorescence quenching of CdqCl nanowires are due to two quenchers present in concentrations $[Q]_a$ for $AuCl_4^-$ and $[Q]_b$ for generated Au nanoparticles, their contribution to the overall quenching process is given by:

$$\frac{d\left(\frac{F_c}{F}\right)}{d[H_2O_2]} = \frac{d\left(\frac{F_0}{F_a}\right)}{d[Q]_a} + \frac{d\left(\frac{F_0}{F_b}\right)}{d[Q]_b} \quad (2)$$

where F_c is the fluorescence intensity of CdqCl nanowires in the presence of the Au nanoparticles growth solution (containing 2.4×10^{-4} M $AuCl_4^-$, 2.0×10^{-3} M CTAC, 1.8×10^{-6} M Au seeds, 0.01 M PBS, pH 7.05) but without the reducing reagent (H_2O_2). F is the fluorescence intensity of CdqCl nanowires in the presence of the Au nanoparticles growth solution after the addition of reducing reagent H_2O_2 (or H_2O_2 generated by glucose/glucose oxidase). F_0 is the fluorescence intensity of CdqCl nanowires in the presence of a blank solution (containing 2.0×10^{-3} M CTAC, 0.01 M PBS, pH 7.05). F_a is the fluorescence intensity of CdqCl nanowires in the presence of the blank solution with $AuCl_4^-$. F_b is the fluorescence intensity of CdqCl in the presence of the blank solution with Au nanoparticles. $[H_2O_2]$, $[Q]_a$ and $[Q]_b$ are the concentrations of H_2O_2 (or H_2O_2 generated by glucose/glucose oxidase), $AuCl_4^-$, and Au nanoparticles (NPs), respectively. According to the reaction equation

$$AuCl_4^- + 3/2H_2O_2 \xrightarrow{\text{Au NP seeds}} Au^0 + 4HCl + 3/2O_2 \quad (3)$$

$[Q]_a = [Q]_0 - [Q]_b$ and $\Delta[Q] = [Q]_0 - [Q]_a$ are obtained, where $[Q]_0$ is the initial concentration of $AuCl_4^-$: $[Q]_0 = 2.4 \times 10^{-4}$ M. In the case of $AuCl_4^-$ or Au nanoparticles as the single quencher, the corresponding S–V equation can be written as:

$$\frac{d\left(\frac{F_0}{F_a}\right)}{d(\Delta[Q])} = {}^aK_{SV} \quad (4)$$

$$\frac{d\left(\frac{F_0}{F_b}\right)}{d([Q]_b)} = {}^bK_{SV} \quad (5)$$

where ${}^aK_{SV}$ and ${}^bK_{SV}$ are the Stern–Volmer quenching constants of $AuCl_4^-$ and Au nanoparticles, respectively. Substituting $\Delta[Q] = [Q]_0 - [Q]_a$ into Equation 4, we obtain:

$$\frac{d\left(\frac{F_0}{F_a}\right)}{d(\Delta[Q])} = \frac{d\left(\frac{F_0}{F_a}\right)}{d([Q]_0 - [Q]_a)} = \frac{d\left(\frac{F_0}{F_a}\right)}{d([Q]_a)} = {}^aK_{SV} \quad (6)$$

then we get the overall quenching equation from Equations 2, 5, and 6 as:

$$\frac{d\left(\frac{F_c}{F}\right)}{d[H_2O_2]} = {}^bK_{SV} - {}^aK_{SV} \quad (7)$$

Equation 7 shows that the rate of change of total fluorescence intensity depends on the value of $({}^bK_{SV} - {}^aK_{SV})$. In this present work, we get the total quenching constant $K_{SV} = {}^bK_{SV} - {}^aK_{SV} = 7.56 \times 10^3\ M^{-1}$. Mathematically, if $d\left(\frac{F_c}{F}\right)/d[H_2O_2] > 0$, the value of F_c/F decreases with the increase of $[H_2O_2]$. In another word, the CdqCl nanowires fluorescence decreases with the increase of H_2O_2 or glucose. From the S–V plot in Figures 5d and 6d, the total quenching constant for the case of H_2O_2 and glucose were found to be 6.84×10^3 and $6.77 \times 10^3\ M^{-1}$, respectively, which is in good agreement with the results of Equation 7 ($K_{SV} = 7.56 \times 10^3\ M^{-1}$).

3. Conclusions

Well-defined CdqCl complex nanowires were synthesized via a sonochemical route. TEM and SEM images showed that the CdqCl complex was in the form of nanowires with diameter of about 50 nm and length of 2–4 μm. By controlling the ratio of $CdCl_2$/q, the morphology and composition of the products could be transformed from Cdq_2 micrometer sized flakes to CdqCl nanowires. A new fluorescent sensing strategy for detecting H_2O_2 and glucose was developed on the basis of the combination of the luminescent nanowires and the biocatalytic growth of Au nanoparticles. The quenching effects of Au nanoparticles and $AuCl_4^-$ on the fluorescence of CdqCl nanowires were investigated. It was found that the Stern–Volmer quenching constant of Au nanoparticles is larger than that of $AuCl_4^-$, and this is the dominant factor for the fluorescence quenching of CdqCl nanowires.

4. Experimental

In a typical process for the synthesis of CdqCl nanowires, a certain amount of 8-hydroxyquinoline and $CdCl_2 \cdot 2.5H_2O$ was dissolved in an ethanol/water solution (50% v/v, 50 mL). The molar ratio of $CdCl_2 \cdot 2.5H_2O$/8-hydroxyquinoline was 3:1. The solution was then mixed and exposed to ultrasonic irradiation in air for 50 min. Ultrasonic irradiation was accomplished with an ultrasonic probe (Xinzhi Co., Xinzhi, China; 1.2 cm diameter; Ti horn, 20 kHz, 100 W cm^{-2}) immersed directly in the reaction solution. When the reaction finished, a yellowish-green precipitate was obtained. The product was purified by centrifugation–redispersion cycles with water and ethanol and then dried in air at 60 °C. The products were characterized by field-emission scanning electron microscopy (FE-SEM; LEO-1530VP), transmission electron microscopy (TEM; JEOL-JEM 200CX), infrared spectroscopy (IR, Nicolet Nexus 870 FT-IR), elemental analysis (EA, Heraeus CHN-O), atomic absorption spectroscopy (AAS, Hitachi 180-80), and photoluminescence spectroscopy (PL, Hitachi 850). All spectra were collected at room temperature.

Preparation of Au Nanoparticle Seeds: Au nanoparticle seeds were prepared by using KBH_4 as reductant and stabilized with sodium citrate following the literature [30, 31]. $HAuCl_4$ (5 mL, 1%) and sodium citrate (10 mL, 0.03 M) were added into 250 mL of doubly distilled water and stirred. Then freshly prepared KBH_4 (5 mL, 0.1 M) was added, and the mixture was stirred at room temperature for 24 h. The diameter of the Au nanoparticle seeds was about 4–7 nm.

Growth of Au Nanoparticles and Fluorescence Sensing for H_2O_2 and β-Glucose: A 5 mL volume of the Au nanoparticles growth solution consisted of 2.4×10^{-4} M $HAuCl_4$, 2.0×10^{-3} M cetyltrimethylammonium chloride (CTAC) in 0.01 M phosphate-buffered saline (PBS), pH 7.05, and different concentrations of either H_2O_2, β-glucose

together with 47 μg mL^{-1} GOx. For the catalytic growth of Au nanoparticles, 20 μL of Au nanoparticle seeds (4.5×10^{-4} M) were added to the growth solution. The growth of Au nanoparticles was performed at a temperature of 5 °C for 5 h in the case of H_2O_2, or 37 °C for 5 h in the case of β-glucose with GOx. Then 15 μL of cysteamine was added to terminate the reaction. Subsequently, 1 mL of CdqCl nanowires (12 mg dispersed in 60 mL doubly distilled water, containing 600 μL 0.2 M CTAC, 2.4 μL 3-mercaptopropionic acid (MPA)) was added into the solution and the fluorescence spectra were recorded after 5 min at room temperature.

Received: April 10, 2008
Revised: June 26, 2008
Published online: November 4, 2008

[1] R. Pohl, P. Anzenbacher, *Org. Lett.* **2003**, *5*, 2769.
[2] M. Braun, J. Gmeiner, M. Tzolov, M. Coelle, F. D. Meyer, W. Milius, H. Hillebrecht, O. Wendland, J. U. von Schütz, W. Brütting, *J. Chem. Phys.* **2001**, *114*, 9625.
[3] M. Cölle, J. Gmeiner, W. Milius, H. Hillebrecht, W. Brütting, *Adv. Funct. Mater.* **2003**, *13*, 108.
[4] P. C. P. Hrudey, K. L. Westra, M. J. Brett, *Adv. Mater.* **2006**, *18*, 224.
[5] Y. S. Zhao, C. Di, W. Yang, G. Yu, Y. Liu, J. Yao, *Adv. Funct. Mater.* **2006**, *16*, 1985.
[6] L. S. Sapochak, F. E. Benincasa, R. S. Schofield, J. L. Baker, K. K. C. Riccio, D. Fogarty, H. Kohlmann, K. F. Ferris, P. E. Burrows, *J. Am. Chem. Soc.* **2002**, *124*, 6119.
[7] M. Matsumura, T. Akal, *Jpn. J. Appl. Phys.* **1996**, *35*, 5357.
[8] P. E. Burrows, Z. Shen, V. Bulovic, D. M. McCarty, S. R. Forrest, J. A. Cronin, M. E. Thompson, *J. Appl. Phys.* **1996**, *79*, 7991.
[9] P. E. Burrows, L. S. Sapochak, D. M. McCarty, S. R. Forrest, M. E. Thompson, *Appl. Phys. Lett.* **1994**, *64*, 2718.
[10] Y. Hamada, M. Sano, T. Fujita, Y. Nishio, K. Shibata, *Jpn. J. Appl. Phys.* **1993**, *32*, L514.
[11] C. W. Tang, S. A. VanSlyke, *Appl. Phys. Lett.* **1987**, *51*, 913.
[12] J. E. Knox, M. D. Halls, H. P. Hratchian, H. B. Schlegel, *Phys. Chem. Chem. Phys.* **2006**, *8*, 1371.
[13] J. J. Chiu, C. C. Kei, T. P. Perng, W. S. Wang, *Adv. Mater.* **2003**, *15*, 1361.
[14] J. S. Hu, H. X. Ji, A. M. Cao, Z. X. Huang, Y. Zhang, L. J. Wan, A. D. Xia, D. P. Yu, X. M. Meng, S. T. Lee, *Chem. Commun.* **2007**, 3083.
[15] J. J. Chiu, W. S. Wang, C. C. Kei, C. P. Cho, T. P. Perng, P. K. Wei, S. Y. Chiu, *Appl. Phys. Lett.* **2003**, *83*, 4607.
[16] J. E. Tackett, D. T. Sawyer, *Inorg. Chem.* **1964**, *3*, 692.
[17] R. G. Charles, A. Langer, *J. Phys. Chem.* **1959**, *63*, 603.
[18] W. Chen, Q. Peng, Y. Li, *Cryst. Growth Des.* **2008**, *8*, 564.
[19] T. Gavrilko, R. Fedorovich, G. Dovbeshko, A. Marchenko, A. Naumovets, V. Nechytaylo, G. Puchkovska, L. Viduta, J. Baran, H. Ratajczak, *J. Mol. Struct.* **2004**, *704*, 163.
[20] G. P. Kushto, Y. Iizumi, J. Kido, Z. H. Kafafi, *J. Phys. Chem. A* **2000**, *104*, 3670.
[21] M. A. Beg, A. Ahmad, S. Beg, H. Askari, *J. Solid State Chem.* **1995**, *117*, 416.
[22] O. A. Raitman, E. Katz, I. Willner, V. I. Chegel, G. V. Popova, *Angew. Chem, Int. Ed.* **2001**, *40*, 3649.
[23] Y. Xiao, V. Pavlov, S. Levine, T. Niazov, G. Markovitch, I. Willner, *Angew. Chem, Int. Ed.* **2004**, *43*, 4519.
[24] R. Baron, M. Zayats, I. Willner, *Anal. Chem.* **2005**, *77*, 1566.
[25] M. Zayats, R. Baron, I. Popov, I. Willner, *Nano Lett.* **2005**, *5*, 21.
[26] I. Willner, R. Baron, B. Willner, *Adv. Mater.* **2006**, *18*, 1109.
[27] R. Gill, L. Bahshi, R. Freeman, I. Willner, *Angew. Chem, Int. Ed.* **2008**, *47*, 1676.
[28] C. D. Geddes, *Meas. Sci. Technol.* **2001**, *12*, R53.
[29] P. Yuan, D. R. Walt, *Anal. Chem.* **1987**, *59*, 2391.
[30] N. Zhou, J. Wang, T. Chen, Z. Yu, G. Li, *Anal. Chem.* **2006**, *78*, 5227.
[31] B. D. Busbee, S. O. Obare, C. J. Murphy, *Adv. Mater.* **2003**, *15*, 414.